SUPPORTING INFORMATION

Reactive cysteine in the structural Zn^{2+} site of the C1B domain from PKCα

*Mikaela D. Stewart and Tatyana I. Igumenova**

Department of Biochemistry and Biophysics, Texas A&M University, 300 Olsen Boulevard, College Station, TX 77843-2128.

*Corresponding author: Tatyana I. Igumenova, phone: (979) 845 6312, fax: (979) 845 4946, e-mail: tigumenova@tamu.edu.

S1. Purification protocol for the C1Bα50 and its C151G variant.

Both proteins were expressed as C-terminal fusions with histidine-tagged SUMO. The over-expression was induced by 0.5 mM IPTG for 12 hours at 15 °C. The cells were harvested and lysed at room temperature using B-PER Protein Extraction Reagent (Thermo Scientific). The fusion protein was purified using a HisTrap HP Ni affinity column (GE Healthcare Life Sciences). The fractions containing fusion protein were pooled, and SUMO was cleaved from C1Bα50 or its C151G variant at 25 °C with SUMO protease. The pET28b plasmid carrying the SUMO protease gene was a generous gift from Dr. Pingwei Li (Texas A&M University). The products of SUMO protease cleavage reaction were separated by gel-filtration chromatography using HiPrep 16/60 Sephacryl S-100 column (GE Healthcare Life Sciences) in 50 mM MES at pH 6.5 and 150 mM KCl. The purity of all proteins was assessed using SDS-PAGE.

S2. PAR assay to determine the C1B Zn^{2+} content.

Zinc content of the constructs used in this study was determined spectroscopically using 4-(2-pyridylazo)-resorcinol (PAR) (Fisher Scientific).[1]

To determine the Zn^{2+} content of the intact C1Bα50, C151G, and C1B-C2 constructs, the protein solution was diluted to 2-5 μM in 4 mM hydrogen peroxide (VWR International) and 50 mM Tris buffer (pH 7.5) that was previously ran over the Chelex-100 resin (Sigma) to remove trace metal ions. This solution was incubated at 42 ºC for 50 minutes then cooled to room temperature. PAR was added to a final concentration of 0.1 mM. The increase in absorbance at 500 nm was measured and compared to that of the control sample treated identically but lacking the protein solute. The zinc content was quantified using a standard calibration curve (1-12 μM Zn^{2+} concentration range) under buffer conditions identical to those used for protein samples. Each measurement was repeated at least three times. Our results showed that C1Bα50, C151G, and C1B-C2 released 1.8 ± 0.1, 2.0 ± 0.1, and 2.2 ± 0.1 molar equivalents of zinc, respectively. This is in agreement with the results obtained on the

MBP-C1Bα fusion protein, which released two molar equivalents of zinc when treated with H_2O_2.[2] Our results also demonstrate that coordination to Zn(2) is maintained in C151G throughout purification despite the loss of Cys151Sγ-Zn(2) bond.

To establish if Zn^{2+} is released by C1B upon H_2O_2 treatment at 25 ºC, we carried out PAR assays on the supernatants of NMR samples treated with H_2O_2. After the intensity of the NMR signals had decayed to less than 10% of the original, the supernatant was removed and diluted into the above Tris buffer and 0.1 mM PAR. No additional H_2O_2 was added. The protein concentration was varied such that the zinc released was between 3-12 μM to be within the range of the standard calibration curve. The calibration curve samples consisted of 1-12 μM Zn^{2+} standard solution, the same volume of NMR buffer as the supernatant assays, Tris buffer, and 0.1 mM PAR. After dilution, all the samples were equilibrated for five minutes at room temperature before measuring the absorbance at 500 nm.

S3. Residue-specific signal decay rates for the C151G and C1B-C2 treated with H_2O_2.

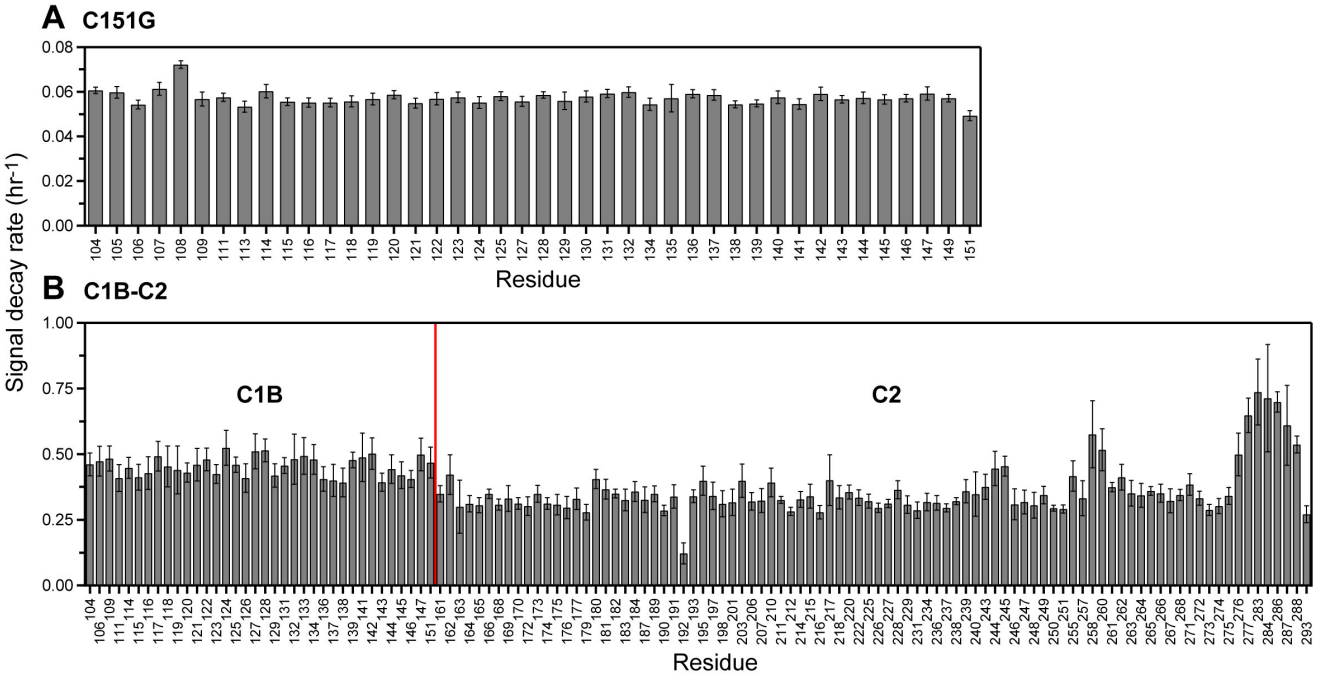

Figure S1. Rates of cross-peak disappearance as a result of (A) C151G and (B) C1B-C2 treatment with H_2O_2.

The mean signal decay rates (per hour) and the standard deviations are:

0.45 (SD 0.04) C1B in C1B-C2

0.36 (SD 0.10) C2 in C1B-C2

0.06 (SD 0.01) C151G

Small differences between the signal decay rates of the C1B and C2 domains in the C1B-C2 construct likely originate from the differences in the domain dynamics in the context of high-molecular weight aggregates.

S4. Reaction of C1B-containing protein constructs with iodoacetamide (IAC).

To alkylate the reactive cysteines, [U-^{15}N]-enriched C1Bα50, C151G, and C1B-C2 were treated with IAC at 10 times the cysteine concentration for one hour in the dark at room temperature before quenching the reaction with dithiothreitol. The final concentration of IAC in the NMR samples was 6, 6, and 12 mM for the C1Bα50, C151G, and C1B-C2 constructs, respectively. ^{15}N-^{1}H heteronuclear single-quantum coherence (HSQC) experiments were recorded to evaluate the state of the protein samples.

The NMR spectra are shown in **Figure S2**. The treatment of C1Bα50, C151G, and C1B-C2 with IAC resulted in the appearance of N-H_N cross-peaks with narrow $^{1}H_N$ chemical shift dispersion. This spectroscopic signature is characteristic for intrinsically disordered and unfolded proteins. No cross-peaks corresponding to the folded C1B were present after the reaction of C1Bα50 (**Figure S2A,** black) and C1B-C2 (**Figure S2B,** orange) with IAC. In contrast, the population of the fully folded protein was still present in the C151G after the IAC treatment (**Figure S2A,** red). We concluded that while all three protein constructs have one or more reactive cysteines whose alkylation results in the loss of native structure of C1B, the presence of Cys151 in the protein (C1Bα50 and C1B-C2) makes it more susceptible to such a reaction.

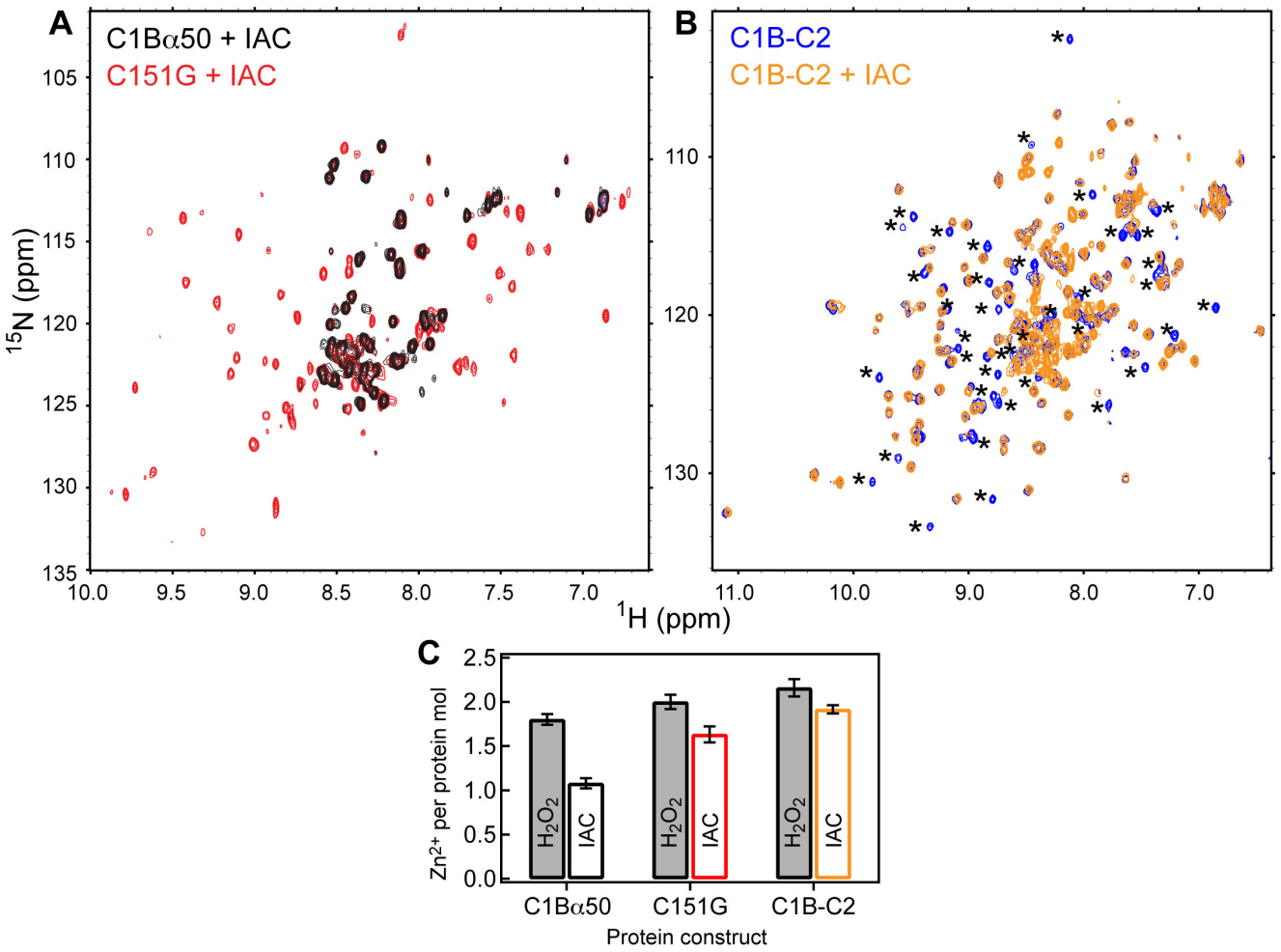

Figure S2. (A) Overlay of the ^{15}N-^{1}H HSQC spectra of the IAC-treated C1Bα50 (black) and C151G (red). (B) Overlay of the ^{15}N-^{1}H HSQC spectra of the native (blue) and IAC-treated C1B-C2 (orange). Cross-peaks labeled with asterisks correspond to the C1B domain in the native C1B-C2 construct. Upon IAC treatment, these cross-peaks shift to the central region of the spectrum. (C) The number of Zn^{2+} ions released per protein molecule in IAC-treated NMR samples (open bars) and H_2O_2-treated samples under conditions favoring full Zn^{2+} release (4 mM H_2O_2 at 42 ºC for one hour)(shaded bars).

S5. Determination of histidine pKa values in C1Bα50.

Figure S3 shows the pH titration curves for three histidine side-chains: His107, His117, and His127 constructed based on the pH response of the ^{15}N and $^{1}H_N$ amide chemical shifts. The curves were fitted with a single pKa equation as described in the manuscript. The pKa values are 6.7 ± 0.1 (His107), 5.6 ± 0.1 (His117), and 6.1 ± 0.1 (His127).

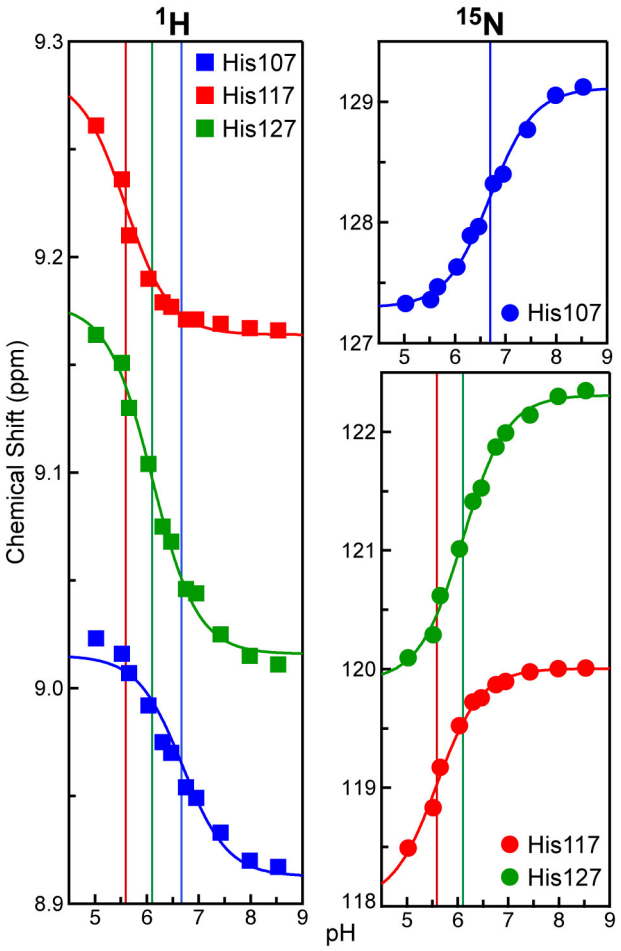

Figure S3. ^{1}H and ^{15}N-detected pH titration curves of His107, His117, and His127 and the corresponding pKa values.

S6. The apparent pKa values of His102 and His140 side-chains are < 5.

The amine group of the N-terminal His102 could not be detected in the ^{15}N-^{1}H HSQC spectra. To probe the pKa values of the His side-chains that are involved in Zn^{2+} coordination, we carried out the "fast" HSQC (fHSQC) experiment[3] with an evolution delay of 22 ms.[4] This delay selects for the two- and three-bond N-H correlations of the histidine side-chains, while suppressing one-bond N-H correlations.

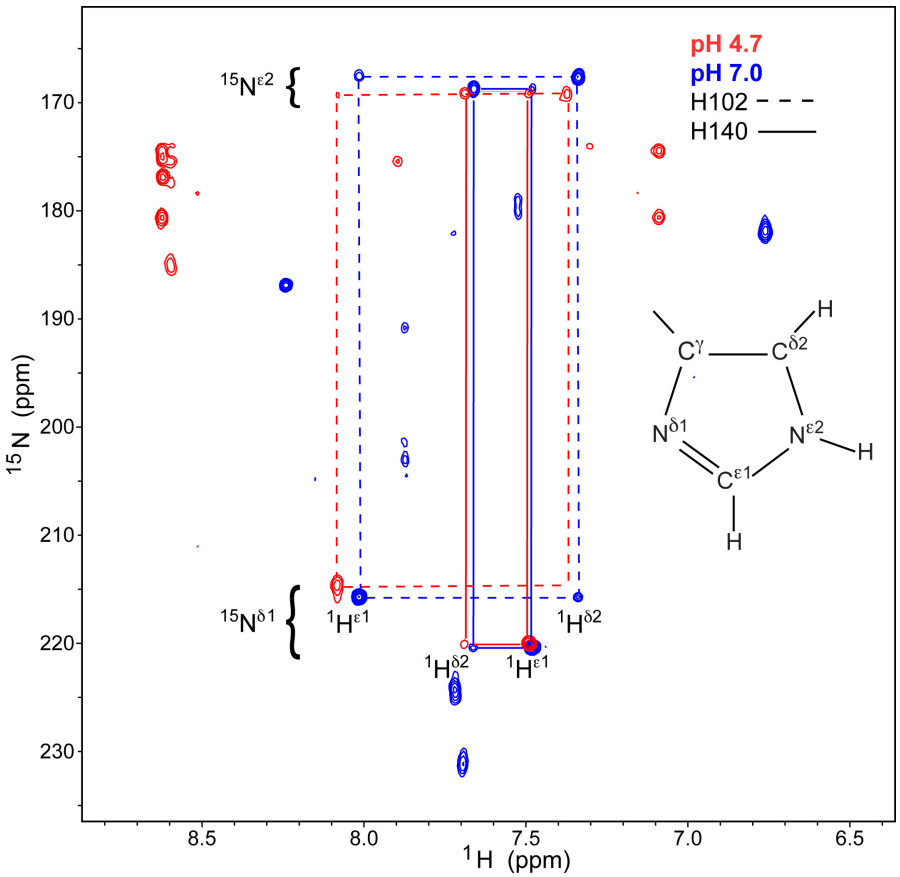

Nucleus	His102		His140	
	pH = 4.7	pH = 7.0	pH = 4.7	pH = 7.0
$^{15}N^{\delta 1}$	215.1	216.2	220.6	220.9
$^{15}N^{\varepsilon 2}$	168.9	167.2	168.8	168.4
$^{1}H^{\delta 2}$	7.37	7.34	7.69	7.66
$^{1}H^{\varepsilon 1}$	8.09	8.02	7.49	7.48

Figure S4. Overlay of the C1Bα50 ^{15}N-^{1}H fHSQC spectra at pH 7.0 (blue) and 4.7 (red). The cross-peaks corresponding to the side-chains of the Zn^{2+}- coordinating histidines H102 and H140 are connected with dashed and solid lines, respectively. The chemical shifts are summarized in the table.

The results are shown in **Figure S4**. The two histidines that are not sensitive to the changes in pH are the ones involved in Zn^{2+} coordination: His102 and His140. The $H^{\delta 2}$ protons of histidine side-chains were assigned using the 2D (HB)CB(CGCD)HD experiment.[5] For both histidines, the pattern of cross-peak intensities in the spectra of **Figure S4** is consistent with a tautomeric state having a de-protonated $N^{\delta 1}$.[6] These data are in agreement with the available structural information on C1Bα.[7] The chemical shifts of $N^{\delta 1}$ and $N^{\varepsilon 2}$ nuclei fall within the range observed for Zn^{2+}-coordinated histidines.[8] Small differences in nitrogen and proton chemical shifts of His102 and His140 at high and low pH are attributed to the transition of conformer *a* at pH 4.7 to conformer *b* at pH 7.0. No large-scale changes indicative of the side-chain protonation/de-protonation events are evident in the spectra. Our data demonstrate that in the range of pH values from 4.7 to 7.0, His102 and His140 remain coordinated to Zn^{2+}, even when Cys151 looses its coordination bond with Zn(2). The apparent pKa values of His102 and His140 are less than 4.7. One of the first examples of this behavior – depression of His side-chain pKa_{app} values due to Zn^{2+} ion coordination – was reported in 1978 for β-lactamase.[9]

S7. Table S1. Summary of fitting results for residues responding to pKa 7.1-7.2.

Residue	*pKa, C1Bα50 b*	*pKa, C151G*
K103	7.2 ± 0.1	7.2 ± 0.1
F104	7.2 ± 0.1	7.1 ± 0.1
T134	7.4 ± 0.1 5.4 ± 0.1[a]	7.0 ± 0.1
C135	7.0 ± 0.1	7.0 ± 0.1
V147	7.4 ± 0.1 5.6 ± 0.1[a]	7.2 ± 0.1 5.4 ± 0.1[a]
L150	7.2 ± 0.1	7.2 ± 0.1

[a]We attribute the second pKa to the ionization of His117 side-chain. His117 side-chain is in close proximity to V147; it is not clear from purely structural considerations why the ^{15}N nucleus of T134 in the *b* conformer of C1Bα50 responds to His117.

S8. Temperature coefficients of C1Bα50 amide protons.

^{15}N-^{1}H HSQC spectra of C1Bα50 collected at 9.4, 15.0, 19.8, 25.0, 30.2, and 35.4 ºC are overlaid in **Figure S5**. The temperature coefficients of $^{1}H_N$ calculated from those spectra ranged from -15.5

(Ile145*a*) to 0.2 (His117) ppb/K. According to the previous reports, the coefficients more positive than -4.5[10] or -5 ppb/K[11] are typical for amide protons engaged in hydrogen-bonding interactions. Ser149 is the only residue in C1Bα50*a* and C1Bα50*b* that crosses the -5 ppb/K "cutoff": its temperature coefficient changes from -4.3 ppb/K in conformation *b* to -8.8 ppb/K in conformation *a*. The amide group of Ser149 does not have any hydrogen-bonding partners in the C1Bα structure. We conclude from our data that the loss of Cys151Sγ–Zn(2) coordination bond does not significantly alter the hydrogen-bonding network of C1Bα50.

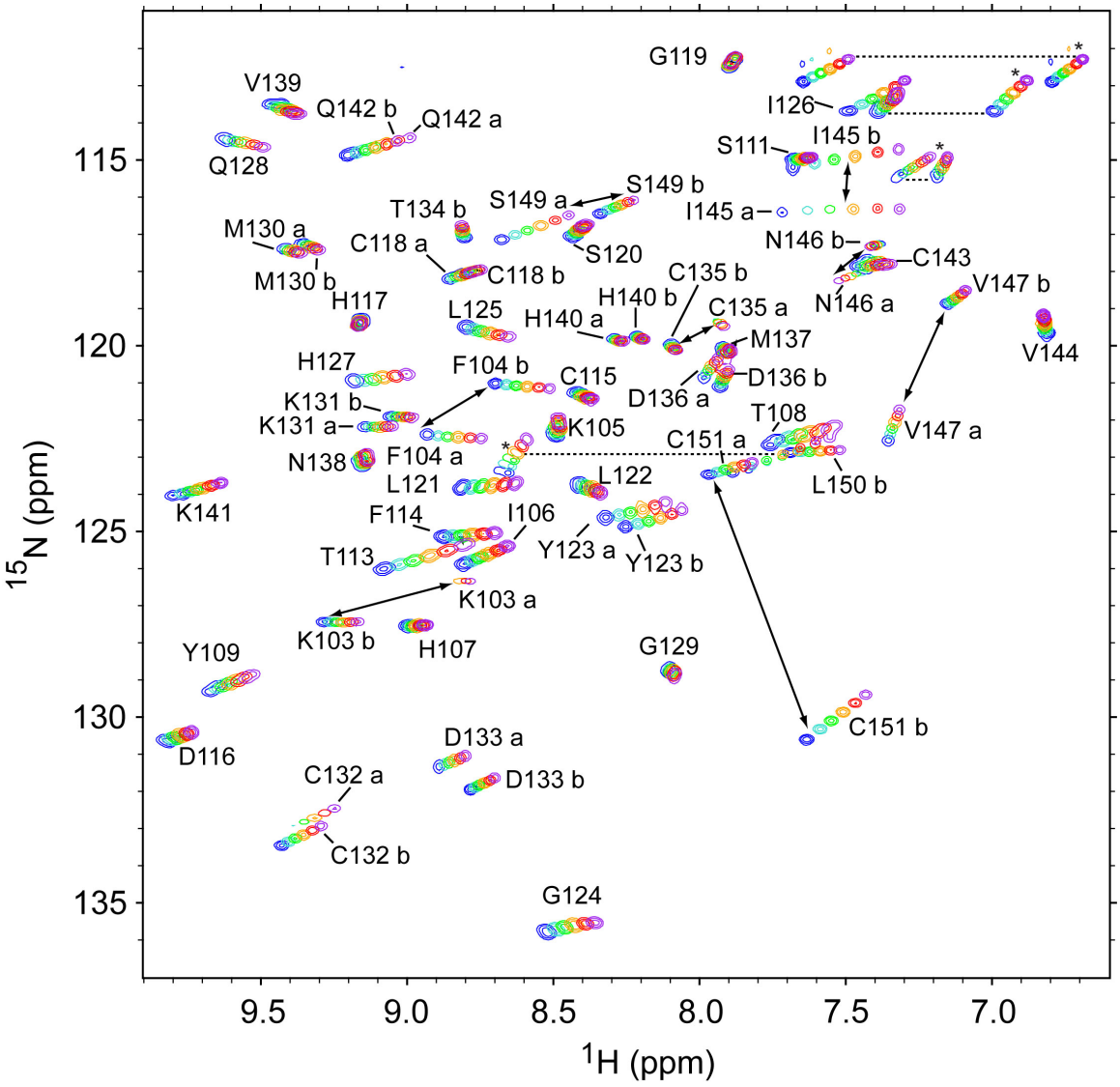

Figure S5. An overlay of C1Bα50 HSQC spectra at increasing temperatures from 9.4 (blue) to 35.4 ºC (magenta) in 5º increments.

S9. RDC-driven refinement procedure.

The first structure of the 2ELI conformational ensemble was taken as a starting model. All RDC values were scaled to $^1D_{NH}$ to take into account the differences in bond lengths and gyromagnetic ratios of the nuclei involved. In addition, the force constants used for different RDC types were scaled to the $^1D_{NH}$ force constant according to the inverse of the relative experimental error ratios squared. These calculations resulted in the following scaling factors for the force constants: $^1D_{NH}$=1 (by default), $^1D_{C\alpha H\alpha}$=2.104, $^1D_{NCO}$= 0.238, and $^2D_{HNCO}$= 0.151. The (ϕ, ψ) dihedral angles and 80 long range NOEs from the 2ELI NMR restraint deposit file in the Protein Data Bank were used as additional restraints. Long-range NOEs were defined as those separated in primary structure by two or more residues, and were only used if both residues *did not* have significantly different RDC values or chemical shifts in the two conformations. Additionally, 6 backbone hydrogen-bonds were identified using WHATIF[12] and used in refinement. The zinc coordination restraints differed for conformers *a* and *b*. For C1Bα50*b,* the distances from the zinc atoms to the coordinating atoms were restrained to 2.3 Å and 2.5 Å for nitrogen and sulfur, respectively, in tetrahedral coordination geometry. For C1Bα50*a,* the distance and angles involving the S_γ of Cys151 in the zinc coordination sphere were not restrained due to the thiolate protonation at low pH. All other zinc-coordinating residues were restrained with the same distances and geometry as for conformation *b*. Because TALOS dihedral angle predictions for residues with different RDC values in conformers *a* and *b* did not make a significant difference in the final structure of *a*, we used the NMR structure-derived angles for the first step of the refinement.

The overall refinement protocol was as reported by Chou and Bax with minor modifications.[13] The parameters are summarized in **Table S2**. The axial (D_a) and rhombic (R_h) components of the alignment tensor were allowed to vary during the minimization steps. Two high-temperature and one low-temperature simulated annealing steps were carried out. The final values for the tensor components were: D_a=7.78(8.06) and R_h=0.54(0.49) for conformer *b*(*a*) in a compressed gel, and D_a=-

22.6(-22.0) and R_h=0.53(0.55) for conformer *b*(*a*) in a stretched gel. The reported structures of *a* and *b* are the regularized average structures determined using the top 5% of the 50 lowest-energy structures obtained in the final refinement step. The lowest-energy structures for conformers *a* and *b* are shown in **Figure S6**.

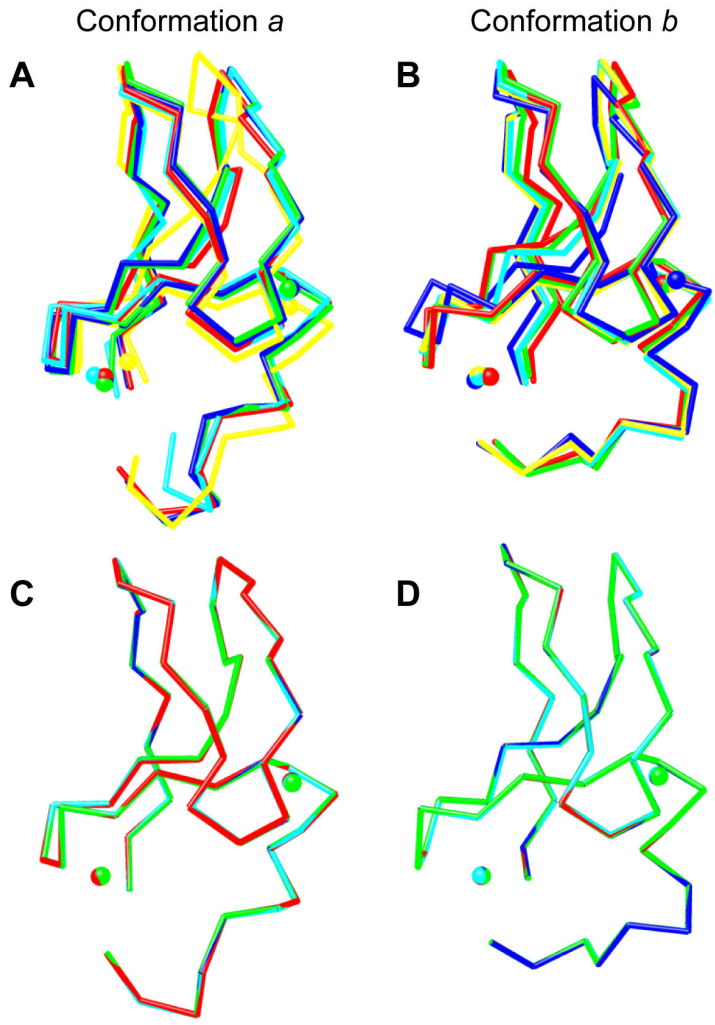

Figure S6. Superposition of the 5 lowest-energy structures for the C1Bα50 conformers *a* and *b* generated as a result of the second high-T annealing step (A and B) and low-T annealing step (C and D). The structures are colored red, blue, green, cyan, and yellow.

Table S2. Parameters of the simulated annealing protocol.

Restraint Type or Parameter	*High Temperature Refinement*	*Low Temperature Refinement*
Temperature	200 → 20 K, DT = 10 K	20 K → 1 K, DT = 1 K
Dihedral angles (φ and ψ)	200 kcal mol^{-1} rad^{-2}	200 → 50 kcal mol^{-1} rad^{-2}
RDCs (Normalized to $^1D_{NH}$)	0.0005 → 1.0 kcal mol^{-1} Hz^{-2}	1.0 kcal mol^{-1} Hz^{-2}
Radius of gyration	50 kcal mol^{-1} $Å^{-2}$	50 kcal mol^{-1} $Å^{-2}$
Hydrogen bonds	2 → 20 kcal mol^{-1} $Å^{-2}$	20 kcal mol^{-1} $Å^{-2}$
Ramachandran potential	0.02 → 0.2 unitless	0.2 unitless
Van der Waals radius	0.002 → 4.0 kcal mol^{-1} $Å^{-4}$	4.0 kcal mol^{-1} $Å^{-4}$
Improper angles	0.1 → 1.0 kcal mol^{-1} deg^{-2}	1.0 kcal mol^{-1} deg^{-2}
Bond angles	0.4 → 1.0 kcal mol^{-1} deg^{-2}	1.0 kcal mol^{-1} deg^{-2}
Long-range NOEs	2.0 → 20 kcal mol^{-1} $Å^{-2}$	20 kcal mol^{-1} $Å^{-2}$
Pre-annealing dynamics	10 ps at 200 K, 0.2 K tolerance	10 ps at 20 K, 0.02 K tolerance
Time per temperature step	5.0 ps	5.0 ps

S10. Table S3. Summary of hydrogen bonds with Sγ of Zn^{2+}-coordinating residues serving as an acceptor.

C1Bδ (1PTQ)	*Zinc Site*	*Donor Res. #[a]*	*Res. ID*	*Atom type*	*Acceptor Res. #[a]*	*Res. ID*	*Atom type*	*Both structures (Y/N)?*
	Zn(1)	117	HIS	N	115	CYS	SG	Y
	Zn(1)	118	CYS	N	115	CYS	SG	Y
	Zn(1)	140	HIS	N	115	CYS	SG	Y
	Zn(1)	*118*	*CYS*	*N*	*118*	*CYS*	*SG*	*Y[c]*
	Zn(1)	120	SER	N	118	CYS	SG	Y
	Zn(2)	103	ARG	N	132	CYS	SG	N
	Zn(2)	134	ASP	N	132	CYS	SG	Y
	Zn(2)	135	CYS	N	132	CYS	SG	Y
	Zn(2)	137	MET	N	135	CYS	SG	Y
	Zn(2)	*135*	*CYS*	*N*	*135*	*CYS*	*SG*	*Y[c]*
C1Bα50b								
	Zn(1)	117	HIS	N	115	CYS	SG	Y
	Zn(1)	118	CYS	N	115	CYS	SG	Y
	Zn(1)	119	GLY	N	115	CYS	SG	N
	Zn(1)	140	HIS	N	115	CYS	SG	Y
	Zn(1)	*118*	*CYS*	*N*	*118*	*CYS*	*SG*	*Y[c]*
	Zn(1)	*119*	*GLY*	*N*	*118*	*CYS*	*SG*	*N[c]*
	Zn(1)	120	SER	N	118	CYS	SG	Y
	Zn(2)	135	CYS	N	132	CYS	SG	Y
	Zn(2)	134	THR	OG1	132	CYS	SG	N
	Zn(2)	134	THR	N	132	CYS	SG	Y
	Zn(2)	*135*	*CYS*	*N*	*135*	*CYS*	*SG*	*Y[c]*
	Zn(2)	137	MET	N	135	CYS	SG	Y
	Zn(2)	134	THR	OG1	151	CYS	SG	N

[a]C1Bα residue numbering is used for clarity.
[b]As prescribed by Zhou et al.,[14] hydrogen bonds D—H---A were identified using 4.1 Å cutoff for the distance between the donor (D) and the acceptor (A), and the angular cutoff of > 90° for the ∠(D—H---A).
[c]Small-angle interactions[14] between $(S\gamma)_i$ and $(HN)_i$ and $(HN)_{i+1}$ that do not fit the canonical definition of hydrogen bonds are italicized.

REFERENCES

(1) Hunt, J. B., Neece, S. H., and Ginsburg, A. (1985) The use of 4-(2-pyridylazo)resorcinol in studies of zinc release from Escherichia coli aspartate transcarbamoylase, *Anal. Biochem. 146*, 150-157.

(2) Zhao, F., Ilbert, M., Varadan, R., Cremers, C. M., Hoyos, B., Acin-Perez, R., Vinogradov, V., Cowburn, D., Jakob, U., and Hammerling, U. (2011) Are zinc-finger domains of protein kinase C dynamic structures that unfold by lipid or redox activation?, *Antioxid. Redox Signal. 14*, 757-766.

(3) Mori, S., Abeygunawardana, C., Johnson, M. O., and van Zijl, P. C. (1995) Improved sensitivity of HSQC spectra of exchanging protons at short interscan delays using a new fast HSQC (FHSQC) detection scheme that avoids water saturation, *J. Magn. Reson. B 108*, 94-98.

(4) Schubert, M., Poon, D. K., Wicki, J., Tarling, C. A., Kwan, E. M., Nielsen, J. E., Withers, S. G., and McIntosh, L. P. (2007) Probing electrostatic interactions along the reaction pathway of a glycoside hydrolase: histidine characterization by NMR spectroscopy, *Biochemistry 46*, 7383-7395.

(5) Yamazaki, T., Forman-Kay, J. D., and Kay, L. E. (1993) 2-Dimensional NMR experiments for correlating C-13-beta and H-1-delta/epsilon chemical shifts of aromatic residues in C-13-labeled proteins via scalar couplings, *J. Am. Chem. Soc. 115*, 11054-11055.

(6) Pelton, J. G., Torchia, D. A., Meadow, N. D., and Roseman, S. (1993) Tautomeric states of the active-site histidines of phosphorylated and unphosphorylated IIIGlc, a signal-transducing protein from Escherichia coli, using two-dimensional heteronuclear NMR techniques, *Protein Sci. 2*, 543-558.

(7) Hommel, U., Zurini, M., and Luyten, M. (1994) Solution structure of a cysteine-rich domain of rat protein kinase C, *Nat. Struct. Biol. 1*, 383-387.

(8) Urbani, A., Bazzo, R., Nardi, M. C., Cicero, D. O., De Francesco, R., Steinkuhler, C., and Barbato, G. (1998) The metal binding site of the hepatitis C virus NS3 protease. A spectroscopic investigation, *J. Biol. Chem. 273*, 18760-18769.

(9) Baldwin, G. S., Galdes, A., Hill, H. A., Smith, B. E., Waley, S. G., and Abraham, E. P. (1978) Histidine residues of zinc ligands in beta-lactamase II, *Biochem. J. 175*, 441-447.

(10) Baxter, N. J., and Williamson, M. P. (1997) Temperature dependence of ^{1}H chemical shifts in proteins, *J. Biomol. NMR 9*, 359-369.

(11) Skalicky, J. J., Selsted, M. E., and Pardi, A. (1994) Structure and dynamics of the neutrophil defensins NP-2, NP-5, and HNP-1: NMR studies of amide hydrogen exchange kinetics, *Proteins 20*, 52-67.

(12) Vriend, G. (1990) WHAT IF: a molecular modeling and drug design program, *J. Mol. Graphics 8*, 52-56, 29.

(13) Chou, J. J., Li, S. P., and Bax, A. (2000) Study of conformational rearrangement and refinement of structural homology models by the use of heteronuclear dipolar couplings, *J. Biomol. NMR 18*, 217-227.

(14) Zhou, P., Tian, F., Lv, F., and Shang, Z. (2009) Geometric characteristics of hydrogen bonds involving sulfur atoms in proteins, *Proteins 76*, 151-163.